Nucleon scalar and tensor couplings from lattice QCD at the physical points

Ryutaro Tsuji[1,2,*], *Yasumichi* Aoki[2], *Ken-Ichi* Ishikawa[3], *Yoshinobu* Kuramashi[4], *Shoichi* Sasaki[1], *Eigo* Shintani[4], and *Takeshi* Yamazaki[4,5]
(PACS Collaboration)

[1]Department of Physics, Tohoku University,980-8578,Sendai, Japan

[2]RIKEN Center for Computational Science, 650-0047, Kobe, Japan

[3]Core of Research for the Energetic Universe, Graduate School of Advanced Science and Engineering, Hiroshima University, 739-8526, Higashi-Hiroshima, Japan

[4]Center for Computational Sciences, University of Tsukuba, 305-8577, Tsukuba, Japan

[5]Faculty of pure and Applied Sciences, University of Tsukuba, 305-8571, Tsukuba, Japan

Abstract. We present results for the axial, scalar and tensor isovector-couplings (g_A, g_S and g_T) of the nucleon obtained from 2+1 flavor QCD with the physical light quark masses (M_π = 135 MeV). Our calculations are performed at a single lattice spacing of 0.085 fm, but with two large volumes of (10.9 fm)^4 and (5.5 fm)^4. The configurations are generated by the PACS Collaboration with nonperturbatively $O(a)$ improved Wilson quark action and Iwasaki gauge action. The result of g_A is a good indicator for determination of g_S and g_T with respect to accuracy and precision. Our result of g_A well reproduces the experimental value within a statistical error of less than 2%. As for g_S and g_T, we compute the renormalization constants at the scale of 2 GeV in the $\overline{\text{MS}}$ scheme through the RI/SMOM$_{(\gamma_\mu)}$ intermediate scheme, and then obtain $g_S = 0.927(83)_{\text{stat}}(22)_{\text{syst}}$ and $g_T = 1.036(6)_{\text{stat}}(20)_{\text{syst}}$.

1 Introduction

While the neutron beta decays occur through the weak interaction via the vector and axial-vector channels, other channels would be allowed due to the physics beyond the standard model (BSM). Indeed, the BSM contributions could be detected by the high-precision research of the nucleon isovector matrix elements such as the precision β-decay measurements with cold and ultracold neutrons [1]. The neutron life-time puzzle associated with the axial isovector-coupling (g_A) is possibly one of such example [2]. The discrepancy between the results of beam experiments and storage experiments remains unsolved. This suggests that the scalar and tensor isovector-couplings (g_S and g_T), which are less known experimentally, play important roles to constrain the limit of non-standard interactions mediated by undiscovered gauge bosons in the scalar and tensor channels [3–5].

---

*e-mail: tsuji@nucl.phys.tohoku.ac.jp
Present adress is *RIKEN Center for Computational Science, 650-0047, Kobe, Japan.*

2 Method

The target quantities of this study depend on a renormalization scale. This indicates that the high-precision and high-accuracy calculations by lattice QCD require the statistically and systematically improved *bare matrix elements* and *renormalization constants*. In our computation, the axial, scalar and tensor couplings are calculated by the quark bilinear operator, $O_\Gamma = \bar{\psi}\Gamma\psi$ with $\Gamma = \gamma_5\gamma_i$, 1 and $\gamma_i\gamma_j$ ($i \neq j$), respectively.

2.1 Bare matrix elements

In general, the *bare matrix elements* are evaluated from a ratio $R(t_{op}, t_{sep} = t_{snk} - t_{src})$ of the zero-momentum projected three-point function with a given operator O_Γ inserted at $t = t_{op}$ being subject to a range of $t_{snk} > t > t_{src}$, to the zero-momentum projected two-point function with a source-sink separation (t_{sep}). If the condition $t_{sep} \gg t_{op} - t_{src} \gg 0$ is satisfied, the desired coupling g_O can be extracted from an asymptotic plateau of the ratio in the t_{op}-independent region (plateau method) as

$$R(t_{op}, t_{sep}) \xrightarrow[t_{sep} \gg t_{op} - t_{src} \gg 0]{} g_O + O(e^{-\Delta E(t_{op} - t_{src})}) + O(e^{-\Delta E(t_{sep} - t_{op} + t_{src})}), \tag{1}$$

where $\Delta E = E_1 - E_0$ denotes a difference between the two energies of the ground state (E_0) and the lowest excited state (E_1). Narrower source-sink separation causes systematic uncertainties stemming from the excited-state contaminations represented by two terms of $O(e^{-\Delta E(t_{op} - t_{src})})$ and $O(e^{-\Delta E(t_{sep} - t_{op} + t_{src})})$. The optimal choice of the smearing parameters can help to suppress as much as possible the coefficients of these terms due to the maximal overlap with the ground state.

In this study, we simply focus on the isovector quantities, where the disconnected contributions are canceled by each other under the exact SU(2) isospin symmetry [6]. Therefore, the isovector couplings $g_O = g_O^u - g_O^d$ can be determined only by the connected-type diagrams.

2.2 Renormalization

In order to compare with the experimental values or other lattice results, the bare couplings should be renormalized with the renormalization constants. As for those of the vector and axial-vector currents, $Z_O(O = V, A)$ can be obtained through the Schrödinger functional scheme at vanishing quark masses [7].

For the scalar and tensor cases, we use the Regularization Independent (RI) SMOM$_{(\gamma_\mu)}$ scheme [8–11] as the intermediate scheme in order to evaluate the renormalization constants $Z_O^{RI}(O = S, T)$ in fully nonperturbative manner with help of $Z_O^{SF}(O = V, A)$. For instance, when Z_V^{SF} is used as an input, the renormalization constant for the scalar coupling $Z_S^{RI}(\mu^2)$ can be evaluated by

$$Z_S^{RI}(\mu^2) = Z_V^{SF} \times \frac{\text{Tr}[\Gamma_S \mathcal{P}_S]}{\text{Tr}[\Gamma_V \mathcal{P}_V]} \cdot \frac{\text{Tr}[(\Lambda_V)_B \mathcal{P}_V]|_{\mu^2 = \mu^2(p_1, p_2)}}{\text{Tr}[(\Lambda_S)_B \mathcal{P}_S]|_{\mu^2 = \mu^2(p_1, p_2)}}. \tag{2}$$

The resulting renormalization constants are then converted to the $\overline{\text{MS}}$ scheme at a matching scale μ_0 and evolved to the scale of 2 GeV using the perturbation theory as

$$Z_O^{\overline{\text{MS}}}(2 \text{ GeV}) = E_O(2 \text{ GeV}, \mu_0) \cdot C_O^x(\mu_0) \times Z_O^x(\mu_0) \quad : \quad x \in \left\{ \begin{array}{c} \text{RI/SMOM} \\ \text{RI/SMOM}_{\gamma_\mu} \end{array} \right\}, \tag{3}$$

where the evolusion factor $E_O(2\text{GeV}, \mu_0) = Z_O^{\overline{\text{MS}}}(2 \text{ GeV})/Z_O^{\overline{\text{MS}}}(\mu_0)$ and the conversion factor $C_O^{\text{RI}}(\mu_0) = Z_O^{\overline{\text{MS}}}(\mu_0)/Z_O^{\text{RI}}(\mu_0)$ are computed under the Landau gauge in the perturbation theory.

It is known that the value of $Z_O^{\overline{\text{MS}}}(2 \text{ GeV})$ obtained from $Z_O^{\text{RI}}(\mu_0)$ in Eq.(3) receives the residual dependence on the choice of the matching scale μ_0, even if the resulting constants are evaluated at certaint renormalization scale, and the dependence causes the systematic uncertainties in the determination of the renormalization constants. The major sources of such systematic uncertainties are summarized as following three points: *lattice artifacts*, *unwanted infrared divergence* and *uncertainties from perturbation and others*. In detail, the systematic uncertainties associated with the *lattice artifacts* and *unwanted infrared divergence* which are observed as residual μ_0-dependence are assessed by using two types of fitting forms as

$$f_{\text{Global}}(\mu_0) = \frac{c_{-1}}{(\Lambda_{\text{IR}}^{-1}\mu_0)^2} + c_0 + \sum_{k>0}^{k_{\max}} c_k(a\mu_0)^{2k} \quad \text{and} \quad f_{\text{IR-trunc.}}(\mu_0) = c_0 + \sum_{k>0}^{k_{\max}} c_k(a\mu_0)^{2k} \quad (4)$$

with c_0 being the μ_0-independent value of $Z_O^{\overline{\text{MS}}}(\mu)$. On the other hand, the systematic uncertainties due to *uncertainties from perturbation and others* are estimated by the difference among four choices: the two intermediate renormalization scheme with two ways of estimating the wave function renormalization through Z_V^{SF} or Z_A^{SF}.

3 Simulation details

We mainly use two ensembles of gauge configurations, which are generated by PACS Collaboration with $L^3 \times T = 128^3 \times 128$ and $64^3 \times 64$ lattices using the six stout-smeared [12] $O(a)$-improved Wilson quark action and the Iwasaki gauge action with physical light quarks [13–18] at fixed gauge coupling $\beta = 1.82$ corresponding to the lattice spacing of $a = 0.08520(16)$ fm. Significant reduction of the computational cost is achieved by employing the all-mode-averaging (AMA) [19]. In our computations, we compute the combination of the correlation function with high-precision $O^{(\text{org})}$ and low-precision $O^{(\text{approx})}$ as

$$O^{(\text{AMA})} = \frac{1}{N_{\text{org}}} \sum_{f \in G}^{N_{\text{org}}} \left(O^{(\text{org})f} - O^{(\text{approx})f} \right) + \frac{1}{N_G} \sum_{g \in G}^{N_G} O^{(\text{approx})g}, \quad (5)$$

where the superscripts f, g denote the transformation under the translational symmetry.

The quark propagator is calculated using the exponential smeared source (sink) with the Coulomb gauge fixing. In addition to the exponential source (sink), we also use the gauge-covariant, approximately Gaussian-shaped source (sink) [20] for the $L = 128$ lattice, so as to make sure that there is no dependence on the gauge fixing condition and the excited-state contamination is well controlled on our final results (for details see Ref. [21]). All parameters of adopted sources are chosen to optimize the effective mass plateau for the smear-local case in each of $L = 128$ and $L = 64$ lattices.

Two lattice ensembles are generated with the same lattice spacing, but on different lattice sizes: $L^3 \times T = 128^3 \times 128$ and $64^3 \times 64$ corresponding $(10.9 \text{ fm})^4$ and $(5.5 \text{ fm})^4$ lattice volumes. The smaller volume ensemble is also used for computing the renormalization constants which are known to be less sensitive to the finite volume effect.

4 Numerical results

In this study, we present the results for the renormalized values of the isovector axial, scalar and tensor couplings. All of the *bare matrix elements* are evaluated with both 128^4 and

Table 1: Details of the numerical mesurements: lattice size (L), time separation (t_{sep}), smearing-type and -parameters of the quark operator, the number of measurements for the high- and low-precision computations (N_{org} and N_G), the number of gauge configurations (N_{conf}) and the total number of measurements ($N_{meas} = N_G \times N_{conf}$), respectively.

L	t_{sep}	Smearing-type	Smearing parameters	N_{org}	N_G	N_{conf}	N_{meas}
128	10	Exp.(I)	$(A, B) = (1.2, 0.16)$	1	128	20	2,560
	12			1	256	20	5,120
	14			2	320	20	6,400
	16			4	512	20	10,240
	13	Gauss	$(n_G, w_G) = (110, 8.0)$	1	128	20	2,560
	16			6	450	20	9,000
64	11	Exp.(I)	$(A, B) = (1.2, 0.16)$	4	40	50	2,000
	14			4	64	100	6,400
	12	Exp.(II)	$(A, B) = (1.2, 0.14)$	4	256	100	25,600
	14			4	1,024	100	102,400
	16			4	2,048	100	204,800

64^4 lattices by the plateau method. For the renormalization constants for the scalar and tensor couplings, the RI/SMOM$_{(\gamma_\mu)}$ schemes are employed as the intermediate schemes and then the resulting values are matched into the $\overline{\text{MS}}$ scheme at the renormalization scale of 2 GeV.

4.1 Renormalization

The smaller volume lattice ensemble ($L = 64$) with 101 gauge configurations with the average of multiple sources at each configuration are used for the renormalized constants computations. For the methodology of our computations, the local vector and axial-vector currents are renormalized with the value of $Z_V = 0.9513(76)(1487)$ and $Z_A = 0.9650(68)(95)$ obtained by the SF scheme [22], while the renormalization constants for the scalar and tensor couplings are evaluated with RI/SMOM$_{(\gamma_\mu)}$ scheme as described in Sec.2.

In this study, three sources of the systematic uncertainties are considered. The *lattice artifacts* correspond to variations of the polynomial parts in the fitting forms Eq.(4) and the *unwanted infrared divergence* is estimated as choice of the fit model of the *infrared* region. In addition, the *uncertainties from perturbation and others* are associated with the choice of the the intermediate schemes and ways of evaluating the wave function renormalization.

Our renormalization constants for the scalar and tensor couplings are determined as

$$Z_S^{\overline{\text{MS}}}(2 \text{ GeV}) = 0.9103(31)_{stat}(231)_{syst} \text{ and } Z_T^{\overline{\text{MS}}}(2 \text{ GeV}) = 1.0111(12)_{stat}(192)_{syst}, \quad (6)$$

where the total systematic errors are evaluated as the root-mean-squared sum of the three systematic uncertainties. On these renormalization constants, the error budget is compiled in Table 2. All errors of the renormalization constants become small enough to be comparable to the precision that is reached for the bare couplings with the statistical errors at the 1-2% level, since we use the RI/SMOM$_{(\gamma_\mu)}$ intermediate scheme that can considerably reduce the systematic errors compared to the case of the RI/MOM scheme.

4.2 Renormalized couplings

The renormalized couplings can be evaluated by combining the value of the bare coupling with the renormalization constant as $Z_O \times g_O^{\text{bare}}$. Figure 1 and 2 show the t_{sep} dependence of

Table 2: The error budget for $Z_S^{\overline{\text{MS}}}(2 \text{ GeV})$ and $Z_T^{\overline{\text{MS}}}(2 \text{ GeV})$ with the RI/SMOM$_{\gamma_\mu}$ intermediate scheme.

		Scalar (Z_S)	Tensor (Z_T)
Statistical:		0.34%	0.12%
Systematical:	Choice of scheme ("scheme")	1.49%	1.84%
	Choice of fit model ("model")	1.40%	0.36%
	Variation of fit ("fit")	1.50%	0.32%
Total:		2.56%	1.90%

the axial, scalar and tensor couplings, which are obtained with several different choices of smearing and t_{sep} on two lattice volumes.

In the case of g_A, the results with $t_{\text{sep}} = \{14, 16\}$ agree well with the experimental values regardless of the lattice volumes and the smearing types. This indicates that the condition $t_{\text{sep}} \geq 14$ is large enough to eliminate the excited-state contaminations. For a combined analysis of two lattice volumes, we simply take an average of two results using only the exponential smeared soueces from both 128^4 and 64^4 lattices. The statistical uncertainties are evaluated by the Jackknife method. Our final result of g_A in this study is

$$g_A = 1.288(14)_{\text{stat}}(9)_{Z_A}, \tag{7}$$

where we also include a systematic error stemming from the error of Z_A^{SF}. This result reproduces the experimental value at the precision level of 1%.

On the other hand, there is no distinct t_{sep} dependence in the region of $t_{\text{sep}} \geq 12$ in both cases of g_S and g_T with two smearing types. This means that the excitd-states contaminations are well under control in such t_{sep} region regardless of the smearing types. Therefore, being similar to the combined analysis of g_A, the results using the exponential smeared sources with $t_{\text{sep}} \geq 12$ from both two lattices are used for our final results. The resulting values of g_S and g_T in this study are

$$g_S = 0.927(83)_{\text{stat}}(22)_{Z_S} \qquad \text{and} \qquad g_T = 1.036(6)_{\text{stat}}(20)_{Z_T}, \tag{8}$$

where the second errors are given by the total systematic uncertainties in the determination of the renormalization constants.

The comparison of our renormalized values of g_S (left) and g_T (right) togather with results from the recent lattice QCD calculations is shown in Fig. 3. Our results are obtained solely form the physical point simulations which suffer from large statistical fluctuations. However our statistical and total errors are comparable to the other lattice results due to the statistical improvement of AMA method for the bare matrix elements and the RI/SMOM$_{(\gamma_\mu)}$ scheme for the renormalization. As for g_S, our result is consistent with the trend of the other results. On the other hand, our result of g_T locates slightly higher than other continuum results (green labels), though this discrepancy would be caused by the discretization uncertainty that is not yet accounted in our calculations.

5 Summary

We have evaluated the renormalized values of the axial, scalar and tensor couplings in $2 + 1$ flavor lattice QCD at the physical point. The calculations are carried out with the gauge
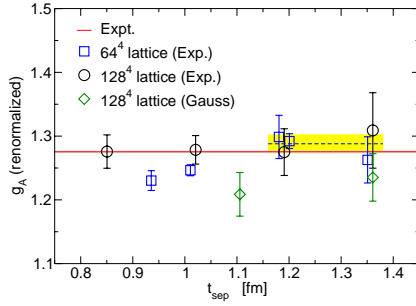
Figure 1: t_{sep} dependence of the renormalized values of g_A. The horizontal axis denotes the source-sink separation t_{sep} in physical unit. Square symbols for the $L = 64$ calculations have been slightly shifted in horizontal direction if they need to avoid overlap. The solid line denotes the experimental value, while the dotted line shows the average value, and shaded band displays the fit range and one standard deviation. This figure is reprinted from Ref. [21].
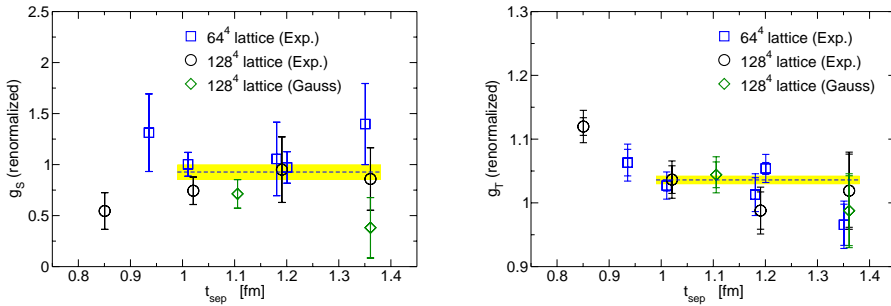

Figure 2: t_{sep} dependence of the renormalized g_S (left) and g_T (right). The horizontal axis denotes the source-sink separation t_{sep} in physical unit. The inner and outer error bars represent their statistical and total uncertainties, respectively. The rest is the same as in Fig. 1. These figures are reprinted from Ref. [21].

configurations generated by the PACS Collaboration with the stout-smeared $O(a)$ improved Wilson quark action and Iwasaki gauge action at a single lattice spacing on the two lattice volumes (linear spatial extents of 10.9 fm and 5.5 fm). In order to acheive high-precision and high-accuracy detemination, we employ the AMA technique which can reduce the statistical noise significantly, and the RI/SMOM$_{(\gamma_\mu)}$ scheme which keeps the systematic error under control in the determination of the renormalization constants. Our final results of g_A is fairly consistent with the experimental results at a percent level of accuracy. As for g_S and g_T, our results are consistent with those of the FLAG average [24], though the discretization uncertainty is not yet accounted in this study. We continue our research to evaluate the systematic uncertainties of g_S and g_T due to the discretization error, using the PACS10 gauge configurations at the finer lattice spacing at the physical point.
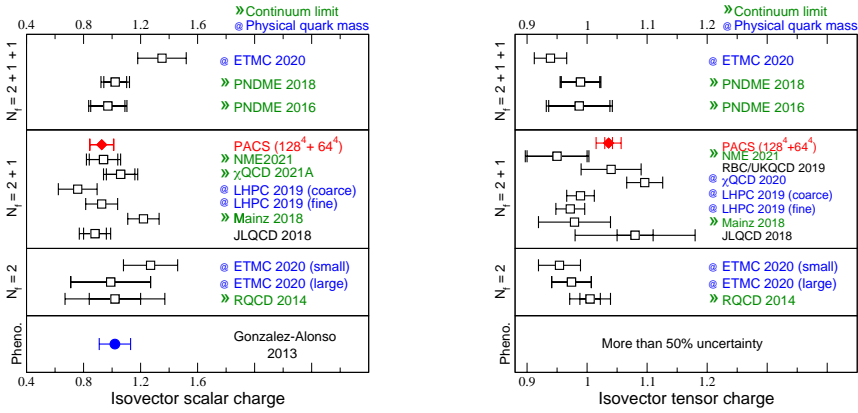
Figure 3: Comparison of our results (red diamonds) with the other lattice results (black squares) [21] and the phenomenological value (blue circle) [23] for g_S (left panel) and g_T (right panel). The inner error bars represent the statistical uncertainties, while the outer ones represent the total uncertainties given by adding the statistical and systematic errors in quadrature. Blue labels indicate that the analysis includes the data from lattice QCD simulations near the physical point, while green labels indicate that the continuum extrapolation is achieved. These figures are reprinted from Ref. [21].

Acknowledgement

References

[1] P. Herczeg, Prog. Part. Nucl. Phys. **46**, 413 (2001)
[2] A. Czarnecki, W.J. Marciano, A. Sirlin, Phys. Rev. Lett. **120**, 202002 (2018), `1802.01804`

[3] T. Bhattacharya, V. Cirigliano, S.D. Cohen, A. Filipuzzi, M. Gonzalez-Alonso, M.L. Graesser, R. Gupta, H.W. Lin, Phys. Rev. D **85**, 054512 (2012), `1110.6448`

[4] V. Cirigliano, S. Gardner, B. Holstein, Prog. Part. Nucl. Phys. **71**, 93 (2013), `1303.6953`

[5] M. González-Alonso, O. Naviliat-Cuncic, N. Severijns, Prog. Part. Nucl. Phys. **104**, 165 (2019), `1803.08732`

[6] S. Sasaki, K. Orginos, S. Ohta, T. Blum (RIKEN-BNL-Columbia-KEK), Phys. Rev. D **68**, 054509 (2003), `hep-lat/0306007`

[7] M. Lüscher, S. Sint, R. Sommer, H. Wittig, Nucl. Phys. B **491**, 344 (1997), `hep-lat/9611015`

[8] G. Martinelli, C. Pittori, C.T. Sachrajda, M. Testa, A. Vladikas, Nucl. Phys. B **445**, 81 (1995), `hep-lat/9411010`

[9] Y. Aoki, PoS **LAT2009**, 012 (2009), `1005.2339`

[10] Y. Aoki et al., Phys. Rev. D **78**, 054510 (2008), `0712.1061`

[11] C. Sturm, Y. Aoki, N.H. Christ, T. Izubuchi, C.T.C. Sachrajda, A. Soni, Phys. Rev. D **80**, 014501 (2009), `0901.2599`

[12] C. Morningstar, M.J. Peardon, Phys. Rev. D **69**, 054501 (2004), `hep-lat/0311018`

[13] Y. Iwasaki (1983), `1111.7054`

[14] K.I. Ishikawa, N. Ishizuka, Y. Kuramashi, Y. Nakamura, Y. Namekawa, E. Shintani, Y. Taniguchi, N. Ukita, T. Yamazaki, T. Yoshié (PACS), Phys. Rev. D **100**, 094502 (2019), `1907.10846`

[15] E. Shintani, K.I. Ishikawa, Y. Kuramashi, S. Sasaki, T. Yamazaki, Phys. Rev. D **99**, 014510 (2019), [Erratum: Phys.Rev.D 102, 019902 (2020)], `1811.07292`

[16] K.I. Ishikawa, Y. Kuramashi, S. Sasaki, E. Shintani, T. Yamazaki (PACS), Phys. Rev. D **104**, 074514 (2021), `2107.07085`

[17] R. Tsuji, Y. Aoki, K.I. Ishikawa, Y. Kuramashi, S. Sasaki, T. Yamazaki, E. Shintani (PACS), PoS **LATTICE2021**, 504 (2022), `2112.15276`

[18] R. Tsuji, Y. Aoki, K.I. Ishikawa, Y. Kuramashi, S. Sasaki, E. Shintani, T. Yamazaki, *Nucleon isovector tensor charge from lattice QCD with physical light quarks*, in *24th International Symposium on Spin Physics* (2022), `2201.11397`

[19] T. Blum, T. Izubuchi, E. Shintani, Phys. Rev. D **88**, 094503 (2013), `1208.4349`

[20] S. Güsken, Nucl. Phys. B Proc. Suppl. **17**, 361 (1990)

[21] R. Tsuji, N. Tsukamoto, Y. Aoki, K.I. Ishikawa, Y. Kuramashi, S. Sasaki, E. Shintani, T. Yamazaki (PACS), Phys. Rev. D **106**, 094505 (2022), `2207.11914` and references therein.

[22] K.I. Ishikawa, N. Ishizuka, Y. Kuramashi, Y. Nakamura, Y. Namekawa, Y. Taniguchi, N. Ukita, T. Yamazaki, T. Yoshié (PACS), PoS **LATTICE2015**, 271 (2016), `1511.08549`

[23] M. González-Alonso, J. Martin Camalich, Phys. Rev. Lett. **112**, 042501 (2014), `1309.4434`

[24] Y. Aoki et al. (Flavour Lattice Averaging Group (FLAG)), Eur. Phys. J. C **82**, 869 (2022), `2111.09849`